Inverse Design of Thin-Plate Elastic Wave Devices

J.R. Capers*

Centre for Metamaterials Research and Innovation, University of Exeter, Stocker Road, Exeter, EX4 4QL, United Kingdom

(Received 8 June 2023; revised 27 July 2023; accepted 22 August 2023; published 27 September 2023)

Motivated by recent advances in the inverse design of electromagnetic materials, we develop two methods for manipulating flexural waves on thin elastic plates. First, we derive a technique for determining plate pinning or mass loading of a thin plate, designing structures that focus elastic energy or isolate a region of space from vibrations. Taking inspiration from the adjoint method in electromagnetism, we show how to design graded plates to act as lenses or perform mode shaping. Both of the methods presented are simple, versatile, and straightforward to implement, making them useful for designing a wide range of devices for sensing, energy harvesting, and vibration isolation.

DOI: 10.1103/PhysRevApplied.20.034064

I. INTRODUCTION

Controlling mechanical motion is key to many applications such as sensing [1], energy harvesting [2,3], and vibration isolation [4]. Elastic materials can be engineered to support a rich variety of wave-shaping behaviors, from mimicking the dispersion relations of condensed-matter systems [5,6] to exhibiting interesting modal properties [7]. However, few techniques exist to design the properties of elastic systems to manipulate elastic waves in particular ways for particular applications.

While elastic deformations are, in general governed by a set of nonlinear tensorial equations [8], when applied to small deformations of a thin plate, the description simplifies to the Kirchhoff-Love equation [5,9–11]. This linear differential equation, a combination of Helmholtz and modified Helmholtz equations, governs the transverse displacement of the plate. Here, we use this simplified description of elastic waves and ask the question "At what points to pin or mass load a plate in order to manipulate the waves propagating on it in a particular way?" Several methods have been developed to answer this question. Traditional least-squares fitting techniques have been utilized to design "metaclusters" of mass-loaded points that scatter flexural waves into particular angles [10] and analytic methods have been employed to design elastic diffraction gratings [12]. For energy-harvesting applications, methods utilizing adiabatic grading [3,13] or exploiting disorder [14] have enabled the design of devices that focus energy to particular points in space. Machine learning has also been employed to manipulate the properties of edge modes by engineering the unit cell [15].

In addition to pinning or mass loading plates, grading the properties of the plates in space can change how the mechanical waves propagate. By analogy with results in transformation optics [16], coordinate mappings can be used to design invisibility cloaks [17–25] for elastic waves on thin plates. Taking ideas from electromagnetism, graded-index lenses for elastic waves have been realized in many ways, including grading plate thickness in space or distributing rods of differing radius in space [26]. By grading the height of a thin plate in space, one can realize Luneburg, Eaton, and Maxwell fish-eye lenses [27] for elastic waves. Despite great progress in designing elastic materials to manipulate mechanical waves, there remains the opportunity to develop more versatile inverse design techniques.

In this work, we develop two perturbative techniques for structuring thin plates to manipulate flexural waves. In Sec. II, we apply the methods presented in Refs. [28,29] to design quasidisordered arrangements of pinned points that can focus flexural waves or isolate regions of space from vibration. Then, in Sec. III, we take inspiration from the adjoint method in electromagnetism [30] to grade the properties of thin plates in space to achieve both lensing and mode shaping. Being both simple and numerically efficient, the techniques we develop may find utility in a range of applications from energy harvesting to sensing.

*j.capers@exeter.ac.uk

II. QUASIDISORDERED ARRANGEMENTS OF PINNED POINTS

We begin by developing a method to design quasidisordered arrangements of pinned points. Considering a plate of thickness h supporting waves of wavelength λ, when $h \ll \lambda$, time-harmonic flexural waves on the plate obey the following equation [8]:

$$\left(\nabla^4 - k_0^4\right)\phi(\mathbf{r}) = 0, \tag{1}$$

where $k_0^4 = h\omega^2\rho/D$ and, for convenience, we have introduced the flexural rigidity $D = Eh^3/12(1-\nu^2)$. The displacement of the plate in the transverse direction is $\phi(\mathbf{r})$, with the mechanical properties of the plate expressed through the Young's modulus E and the Poisson ratio ν. Under a point excitation at position $\mathbf{r}'$, Eq. (1) can be solved in terms of the Green's function, defined as the solution to

$$\left(\nabla^4 - k_0^4\right)G(\mathbf{r},\mathbf{r}') = \delta(\mathbf{r}-\mathbf{r}'), \tag{2}$$

and given by [31]:

$$G(\mathbf{r},\mathbf{r}') = \frac{i}{8k_0^2}\left[H_0^{(1)}(k_0|\mathbf{r}-\mathbf{r}'|) - H_0^{(1)}(ik_0|\mathbf{r}-\mathbf{r}'|)\right], \tag{3}$$

where $H_0^{(1)}(z)$ is the Hankel function of the first kind. If many point scatterers, e.g., pinning positions or mass loading points, are located at positions $\{\mathbf{r}_n\}$, with scattering strength $\alpha\phi(\mathbf{r}_n)$, then the governing equation [Eq. (1)] acquires source terms of the form

$$\left(\nabla^4 - k_0^4\right)\phi(\mathbf{r}) = \sum_n \alpha\delta(\mathbf{r}-\mathbf{r}_n)\phi(\mathbf{r}_n). \tag{4}$$

This can be directly solved using the Green's function given in Eq. (3), with the solution being

$$\phi(\mathbf{r}) = \phi_{\text{inc}}(\mathbf{r}) + \sum_n \alpha G(\mathbf{r},\mathbf{r}')\phi(\mathbf{r}_n), \tag{5}$$

where $\phi_{\text{inc}}(\mathbf{r})$ is an incident field. Physically, the point scatterers we are describing could be various arrangements of masses and springs attached to the plate. Different configurations of masses and springs are described by different models of α [12,32], with the mass-spring system introducing resonances. In this work, we take the limit of $\alpha \to \infty$, corresponding to pinning the plate in certain locations, i.e., $\phi(\mathbf{r}_n) = 0$. In order to include all multiple-scattering effects in the field applied to each scatterer $\phi(\mathbf{r}_n)$, a self-consistency condition must be imposed [33]. Taking as the unknown $\alpha\phi(\mathbf{r}_n)$, self-consistency results in the matrix equation

$$\mathbf{R}\boldsymbol{\phi}_n = \boldsymbol{\phi}_{i,n}, \tag{6}$$

where $\boldsymbol{\phi}_n = \alpha\phi(\mathbf{r}_n)$, $\boldsymbol{\phi}_{i,n} = \phi_{\text{inc}}(\mathbf{r}_n)$ and the matrix $\mathbf{R}$ is given by

$$R_{ij} = \frac{\delta_{ij}}{\alpha} - G(\mathbf{r}_i,\mathbf{r}_j). \tag{7}$$

Together, the solution to the wave equation [Eq. (5)] and the self-consistency condition [Eq. (6)] allow for the efficient calculation of the displacement of the plate, with many pinned points acting as scatterers.

We now aim to answer the question "Where should the plate be pinned to manipulate flexural waves in certain ways?" To answer this, we employ the techniques outlined in Refs. [28,29], reformulating the key results so that they are applicable to the problem of thin elastic plates. Starting from an initial configuration of pinned points, we will derive an iterative method for increasing a figure of merit. Asking how a change in the position of a scatterer affects the fields, we perturbatively expand the delta functions in Eq. (4),

$$\delta(\mathbf{r}-\mathbf{r}_n-\Delta\mathbf{r}_n) = \delta(\mathbf{r}-\mathbf{r}_n) - \Delta\mathbf{r}_n\cdot\nabla\delta(\mathbf{r}-\mathbf{r}_n) + \ldots, \tag{8}$$

as well as the field $\phi \to \phi + \delta\phi$. Utilizing the properties of the delta function acted upon by a derivative [34], we collect first-order terms to obtain

$$\delta\phi(\mathbf{r}) = -\alpha G(\mathbf{r},\mathbf{r}_n)\Delta\mathbf{r}_n\cdot\nabla\phi(\mathbf{r}_n). \tag{9}$$

This expression connects a small change in the position of a scatterer to a small change in the fields, making it useful for finding an analytic expression for the gradient of a figure of merit. To illustrate this, let us say that we would like to make the displacement large at a particular point $\mathbf{r}_\star$. The figure of merit is therefore

$$\mathcal{F} = |\phi(\mathbf{r}_\star)|^2. \tag{10}$$

Expanding this under small changes in the field, to first order we find

$$\mathcal{F} + \delta\mathcal{F} = |\phi(\mathbf{r}_\star) + \delta\phi(\mathbf{r}_\star)|^2, \tag{11}$$

$$= (\phi^*(\mathbf{r}_\star) + \delta\phi^*(\mathbf{r}_\star))(\phi(\mathbf{r}_\star) + \delta\phi(\mathbf{r}_\star)), \tag{12}$$

$$= |\phi(\mathbf{r}_\star)|^2 + 2\text{Re}[\phi^*(\mathbf{r}_\star)\delta\phi(\mathbf{r}_\star)] + \mathcal{O}(\delta\phi^2). \tag{13}$$

Substituting Eq. (9) to connect the field change to the change in the position of a scatterer, we find an analytic

approximation to the gradient of the figure of merit:

$$\frac{\partial \mathcal{F}}{\partial \mathbf{r}_n} = -2\mathrm{Re}\left[\phi^*(\mathbf{r}_\star)\alpha G(\mathbf{r}_\star, \mathbf{r}_n)\nabla\phi(\mathbf{r}_n)\right]. \quad (14)$$

This expression can be combined with simple gradient-descent optimization to find how to update the positions of the scatterers in order to increase the figure of merit given in Eq. (10), as

$$\mathbf{r}_n^{j+1} = \mathbf{r}_n^j + \gamma \frac{\partial \mathcal{F}}{\partial \mathbf{r}_n^j}, \quad (15)$$

where j is the iteration number and γ is a small step size [35]. Approaching the optimization procedure in this way has a number of important benefits. First, the gradient of the figure of merit with respect to the position of all of the scatterers can be calculated at the same time, making the procedure numerically efficient. Second, while the gradient of the field at each scatterer must be evaluated numerically, the gradient of the figure of merit does not as an analytic expression for it can be derived. An example of utilizing this framework is shown in Fig. 1. Considering flexural waves on a steel plate of thickness $h = 1$ mm at $f = 10$ kHz, we take $E = 100$ GPa, $\sigma = 0.3$ and $\rho = 8000$ kg/m^3. These parameter choices give a wavelength of $\lambda \sim 30$ mm. The initial configuration along with the displacement amplitude $|\phi(\mathbf{r})|$ is shown in Fig. 1(a). A point emitter (red star) is placed next to an ordered array of pinned points (black dots). We aim to increase the displacement amplitude at a target location, indicated by a green cross. Using the gradient we have derived via Eq. (14) along with gradient-descent optimization [Eq. (15)], the scatterers are iteratively moved with the increase in the figure of merit shown in Fig. 1(b). The final pinned-point configuration and displacement amplitude are shown in Fig. 1(c), with a clear peak in amplitude at the desired location. A problem intrinsic to local-optimization techniques, including gradient descent, is the likelihood of finding a local rather than a global optimum. However, the problems we are solving have large search spaces, as a given number of scatterers can be placed at any point in space. As a result, while global-optimization techniques such as the genetic "differential evolution" algorithm [36] explore much more of the search space, a global solution is still not guaranteed. To illustrate this, we consider pinning 20 points to solve the same problem as presented in Fig. 1. Employing the differential-evolution algorithm with a population size of 20, a crossover probability of CR $= 0.7$, and a differential weight parameter of $F = 0.5$, we design the structure shown in Fig. 2(a). To see whether this is a global or local minimum, we use this as the starting point for our gradient-descent optimization technique. The progress of the optimization and the result are shown in Figs. 2(b) and 2(c), respectively. Our method enhances the figure of merit by a factor of approximately 3, meaning that the genetic algorithm did not find a global optimum. We conclude that due to the size of the search space, our method is unlikely to find a global optimum; however, other methods would also be unable to guarantee this.

Taking these ideas further, we can design a structure that couples a point emitter to different locations at different frequencies. Multiple figures of merit can be optimized by adding them together in a weighted sum, where the weights depend on the current values of each figure of merit [29]. Now, we seek to simultaneously increase two figures of merit, given by

$$\mathcal{F}_1 = |\phi(\mathbf{r}_1, \omega_1)|^2 \quad \mathcal{F}_2 = |\phi(\mathbf{r}_2, \omega_2)|^2. \quad (16)$$

For our two frequencies, we take 10 kHz and 12 kHz, with the location of the emitter shown as a red star in Fig. 3 and the target locations are green and magenta crosses. Our figure of merit is therefore

$$F = w_1\mathcal{F}_1 + w_2\mathcal{F}_2, \quad (17)$$

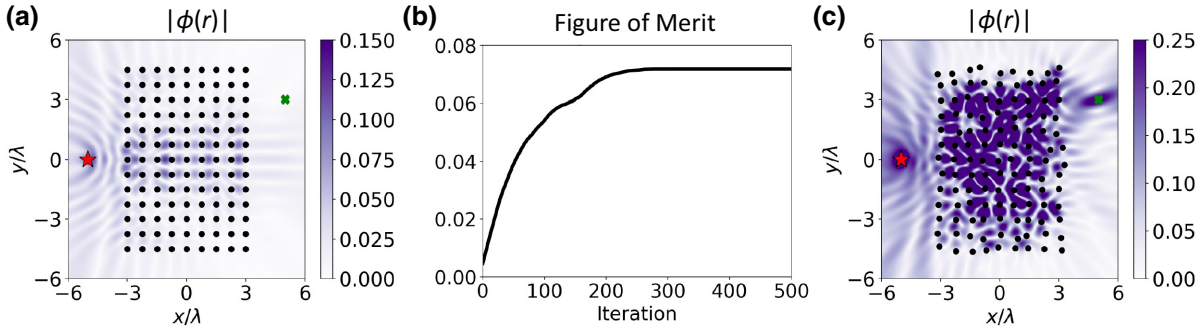

FIG. 1. Iteratively designing a structure of pinned points, with displacement amplitude $|\phi(\mathbf{r})|$, to focus mechanical energy. (a) The initial positions of the points are shown as black dots, while the driving point source is shown as a red star. We seek to focus energy to the green cross. (b) Updating the positions of the scatterers according to the gradient given by Eq. (14), the increase in the figure of merit is shown. (c) The final pinned-point configuration and the displacement amplitude.

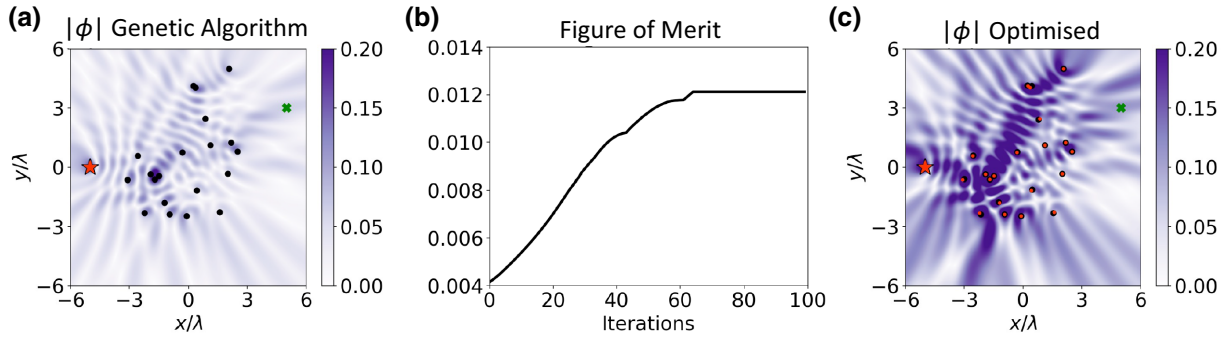

FIG. 2. Comparing our optimization technique to global search methods. (a) Seeking to solve the same problem as in Fig. 1, we design an arrangement of 20 pinned points using the differential evolution genetic algorithm, with displacement amplitude $|\phi|$. To see whether this is a global minimum, we use this structure as the starting point of our gradient descent optimization. (b) The progress of the optimization, showing the figure of merit. (c) The final structure. The black points indicate the pinned locations given by the genetic algorithm, with the red points indicating the optimized pinning locations.

where the weights are chosen to be $w_i \propto 1/\mathcal{F}_i$ and normalized such that $\sum_i w_i = 1$. Since we seek to maximize the figure of merit, this choice ensures that if a figure of merit begins small, its weight will be large so the optimization will favorably enhance it. Overall, choosing the weights in this way seeks to ensure that both figures of merit in the sum given in Eq. (17) have similar values at the end of the optimization. The progress of the optimization is shown in Fig. 3(a), with the displacement amplitude at 10 kHz and 12 kHz shown in Figs. 3(b) and 3(c), respectively. The result is a single passive structure that performs different operations at different frequencies.

As a final example of the flexibility of this method, we consider trying to isolate a region of space. We attempt to design a structure that has a region where the flexural waves do not penetrate, so that whatever is placed there has no effect on the scattering, as it is completely isolated. Starting from an ordered structure of pinned points, under plane-wave incidence $\phi_{\text{inc}} = \exp(ikx)$, we consider a circular region of radius $r = 2\lambda$ centered at the origin, which is to be isolated. This setup and the displacement amplitude are shown in Fig. 4(a). Our figure of merit to be minimized in this case is

$$\mathcal{F} = \int d^2\mathbf{r}' |\phi(\mathbf{r}')|^2, \tag{18}$$

where the integral is evaluated over the region that we seek to isolate. Expanding this under small changes in the fields and then substituting Eq. (9), we find that the gradient is

$$\frac{\partial \mathcal{F}}{\partial \mathbf{r}_n} = -2 \int d^2\mathbf{r}' \text{Re}\left[\phi^*(\mathbf{r}')\alpha G(\mathbf{r}', \mathbf{r}_n)\nabla\phi(\mathbf{r}_n)\right]. \tag{19}$$

Evaluating the integral numerically, this gradient can be used to design a structure that isolates a small region of space. The progress of the figure of merit given in Eq. (18) over the optimization is shown in Fig. 4(b), with the final structure and displacement amplitude shown in Fig. 4(c).

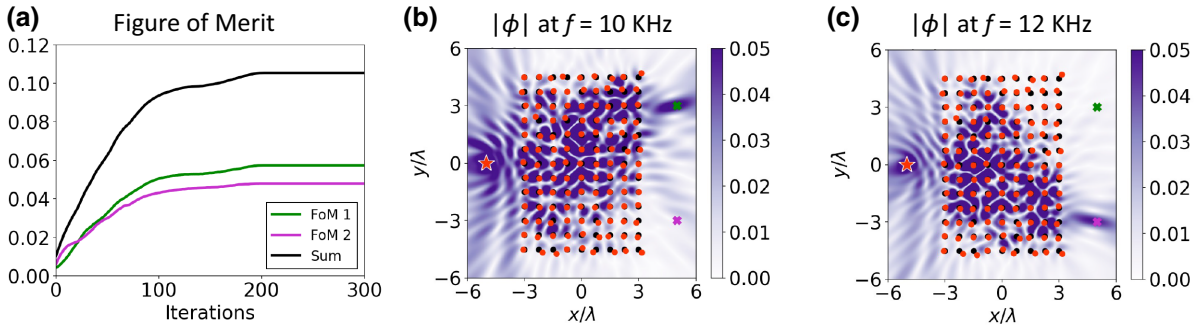

FIG. 3. The design of a frequency-dependent device. We seek to design a structure that is excited by a point source, shown as a red star, at $(-6\lambda, 0)$ and produces amplitude peaks at different places depending on the frequency of operation. (a) Applying our iterative framework, the changes in the figures of merit and their sum are shown. (b),(c) The displacement amplitude of the final device, $|\phi|$, is shown operating at the two design frequencies, (b) 10 kHz and (c) 12 kHz, respectively. The target focus point at 10 kHz is shown as a green cross, while the target point at 12 kHz is indicated by a magenta cross. Initial pinned-point locations are shown as black dots, with the optimized pinned locations shown as red dots.

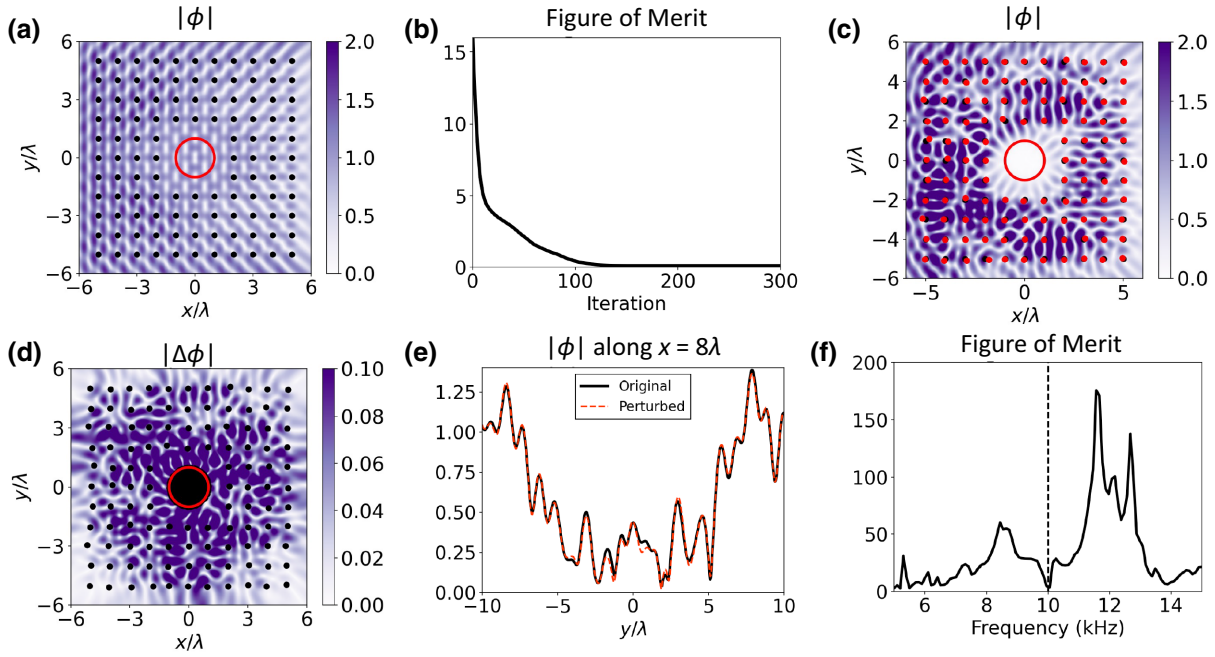

FIG. 4. Designing a device that provides vibration isolation for a small region of space. (a) An initially regular arrangement of pinned points (black dots) under plane-wave incidence has a displacement amplitude $|\phi|$ as shown. We aim to isolate the region of space indicated by the red circle. (b) Updating the pinned locations according to Eq. (19), the decrease in the figure of merit given in Eq. (18) over the optimization is shown. (c) The displacement amplitude $|\phi|$ of the final device, where the optimized pinning locations are shown as red dots. (d) Investigating the behavior of the device, we pin over 1000 points inside the isolated region and then plot the change in the field, $|\Delta\phi|$. (e) Comparing the pinned and unpinned cases along a cut line (i.e., $|\phi|$ along $x = 8\lambda$), we see only small changes in the field. (f) Considering the bandwidth of the device, we see that the best performance in terms of the figure of merit is obtained at the design frequency, with a small bandwidth.

While it is evident from the field in Fig. 4(c) that the region of space that has been targeted is isolated, the performance of the device is considered in Figs. 4(d)–4(f). We consider pinning over 1000 points in the region that we have tried to isolate. If the area is not well isolated, this would significantly affect the scattering. The difference between the field with the region pinned versus unpinned is shown in Fig. 4(d). The difference in the field is about an order of magnitude lower than the field itself. Plotting the field along a cut line at $x = 8\lambda$ when the region is pinned and comparing it to the unpinned case [Fig. 4(e)], only small deviations in the field can be observed. Finally, the bandwidth of the device is considered in Fig. 4(f), by plotting the figure of merit given in Eq. (18) as a function of the frequency. At the design frequency of 10 kHz, the figure of merit is approximately 0.05, although the bandwidth is low at < 1 kHz. Narrow bandwidth is a consequence of the device relying upon many multiple-scattering effects to achieve the desired behavior. If one instead were to attach masses on springs, the resulting resonances might be used to engineer a higher bandwidth by grading the mass-spring properties, as well as their positions, in space. In other contexts, it has been demonstrated that building structures from different species of resonator can enable spectral control (see, e.g., Ref. [37,38]). In the context of the method we have presented here, one could attach mass m_n to the plate with a spring of spring constant k_n. Following Torrent *et al.*, the scattering coefficient for the nth scatterer is then

$$\alpha_n(\omega) = \frac{m_n}{D}\frac{\omega_n^2\omega^2}{\omega_n^2 - \omega^2}, \tag{20}$$

where $\omega_n = \sqrt{k_n/m_n}$ is the resonant frequency of the mass. Our optimization might then be extended to a figure of merit defined over a bandwidth. For example, to extend the bandwidth of the device presented in Fig. 1, one might seek to optimize over a given frequency band

$$\mathcal{F} = \int_{\omega_1}^{\omega_2} d\omega |\phi(\mathbf{r}_\star, \omega)|. \tag{21}$$

Then, as well as moving the locations on the pinned points, one could then find the analytic form of $\partial\mathcal{F}/\partial\omega_n$ and use this to update the resonance frequencies iteratively to attempt to increase the bandwidth.

III. GRADING PLATES

As well as mass loading or pinning, the mechanical properties of the plate itself can alternatively be continuously graded in space [26,27]. In this section, we take

inspiration from the adjoint method in electromagnetism [30] to develop a simple and intuitive framework to design graded plates for a range of applications. While the adjoint method was first developed in structural mechanics [39], it has not been extensively used to design graded elastic systems for wave manipulation. Returning to the wave equation for time-harmonic elastic waves on thin plates,

$$\left(\nabla^4 - \frac{h\omega^2}{D}\rho\right)\phi(\mathbf{r}) = 0, \tag{22}$$

we now consider the effect of grading the properties of the plate in space. For ease of implementation, our optimization grades the mass density ρ in space, although through the dispersion relation this is then converted to a plate height grading. Asking how a small change in mass density produces a small change in the fields, we perturbatively expand the mass density $\rho = \rho + \delta\rho$ and the fields $\phi = \phi + \delta\phi$. To first order, we find that

$$\left(\nabla^4 - \frac{h\omega^2}{D}\rho\right)\delta\phi = \frac{h\omega^2}{D}\phi\delta\rho. \tag{23}$$

This inhomogeneous equation can be solved by integrating the source term against the Green's function [40]:

$$\delta\phi(\mathbf{r}) = \frac{h\omega^2}{D}\int d^2\mathbf{r}' G(\mathbf{r},\mathbf{r}')\delta\rho(\mathbf{r}')\phi(\mathbf{r}'). \tag{24}$$

Assuming that the mass density changes at a single point $\mathbf{r}_i$ by an amount $\Delta\rho$, so that $\delta\rho(\mathbf{r}) = \Delta\rho\delta(\mathbf{r}-\mathbf{r}_i)$, the integral can be easily evaluated to give

$$\delta\phi(\mathbf{r}) = \frac{h\omega^2}{D}G(\mathbf{r},\mathbf{r}_i)\phi(\mathbf{r}_i)\Delta\rho. \tag{25}$$

Just as Eq. (9) allowed us to connect a small change in the position of a pinned point to a change in the fields, this expression allows us to connect a change in the mass density to a change in the fields. As before, we will utilize this to efficiently calculate derivatives of figures of merit. Beginning with the same example as the previous section, we seek to design a graded structure that maximizes $\mathcal{F} = |\phi(\mathbf{r}_\star)|^2$. Expanding under small changes in the field caused by mass-density variations, we find that

$$\delta\mathcal{F} = 2\mathrm{Re}\left[\phi^*(\mathbf{r}_\star)\delta\phi(\mathbf{r}_\star)\right] \tag{26}$$

$$= \frac{2h\omega^2}{D}\mathrm{Re}\left[\phi^*(\mathbf{r}_\star)G(\mathbf{r}_\star,\mathbf{r}_i)\phi(\mathbf{r}_i)\right]\Delta\rho. \tag{27}$$

Exploiting the reciprocity of the Green's function given in Eq. (3) to swap the two arguments and then reordering, we can recast Eq. (27) as

$$\delta\mathcal{F} = \frac{2h\omega^2}{D}\mathrm{Re}\left[\phi(\mathbf{r}_i)G(\mathbf{r}_i,\mathbf{r}_\star)\phi^*(\mathbf{r}_\star)\right]\Delta\rho. \tag{28}$$

This can now be evaluated with only two field calculations. The first is the "forward field" $\phi(\mathbf{r}_i)$, which is the field due to the source evaluated at each of the locations at which we seek to grade the mass density (or height of the plate). The second is the "adjoint field" $G(\mathbf{r}_i,\mathbf{r}_\star)\phi^*(\mathbf{r}_\star)$, which is the field due to a point source at the target location $\mathbf{r}_\star$, evaluated at each point at which we wish to grade the density at $\mathbf{r}_i$, scaled by the value of the field at the target location. In terms of these quantities, the gradient of the figure of merit with respect to the density distribution is given by

$$\frac{\partial\mathcal{F}}{\partial\rho} = \mathrm{Re}\left[\phi(\mathbf{r}_i)\phi_{\mathrm{adjoint}}(\mathbf{r}_i)\right], \tag{29}$$

where the adjoint field is defined as

$$\phi_{\mathrm{adjoint}}(\mathbf{r}) = \frac{2h\omega^2}{D}G(\mathbf{r},\mathbf{r}_\star)\phi^*(\mathbf{r}_\star). \tag{30}$$

The calculation of the displacement of the plate with a graded mass density is facilitated using finite-element simulations in COMSOL MULTIPHYSICS [41]. An illustration of how the adjoint method works is shown in Fig. 5. Seeking to design a graded-density lens for flexural waves, we place a point source at $(-6\lambda, 0)$, generating a field shown in Fig. 5(a). This is our source or "forward" field. Choosing the focus of our lens to be at $(6\lambda, 0)$, we place the adjoint source here, calculating the adjoint field according to Eq. (30), as shown in Fig. 5(b). Multiplying these two fields and then taking the real part, according to Eq. (29), we find the gradient of the figure of merit shown in Fig. 5(c). The region that we will grade is indicated as a black rectangle. The green regions indicate where the mass density should be increased to increase the figure of merit, while the red regions indicate where the mass density should be decreased. An example of using this framework to design a graded lens for waves on elastic plates is shown in Fig. 6. The progression of the figure of merit is shown in Fig. 6(a), with the final structure shown in Fig. 6(b) and the displacement amplitude of the device shown in Fig. 6(d). Considering a slice of the field through the focus, shown in Fig. 6(d), we find that the focal spot has a width of 0.43λ. It can be noted that the final structure shown in Fig. 6(b) does not exactly correspond to the gradient shown in Fig. 5(c). As the optimization iteratively changes the structure, the forwards field $\phi(\mathbf{r}_i)$ that appears in the gradient Eq. (29) changes. As a result, the initial gradient does not exactly resemble the final structure. Lastly, Fig. 6(e) shows the bandwidth of the lens. The peak per-

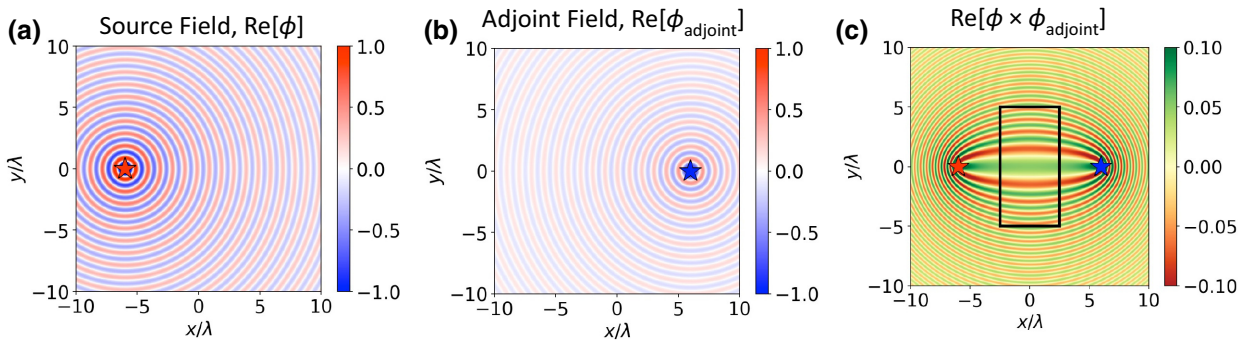

FIG. 5. A schematic of how the adjoint method works. (a) The forward field due to a point source (source field Re[ϕ]) located at the red star. (b) The adjoint field (Re[ϕ_{adjoint}]) is then calculated according to Eq. (30), corresponding to a point source located at the blue star. (c) Interfering these two fields (Re[$\phi \times \phi_{\text{adjoint}}$]), we obtain how to increase or decrease the mass density to increase the figure of merit. The red regions indicate where the mass density should be decreased and the green regions indicate where it should be increased. The region of space that we will grade is indicated by the black rectangle.

formance is at 10 kHz, the design frequency, although the device functions well over a much larger bandwidth than the devices based on multiple scattering of pinned points in the previous section.

The adjoint method can also be leveraged to choose the exact distribution of the field in space. Let us say that we have a one-dimensional line in space on which we would like to choose the shape of the displacement amplitude. The figure of merit we must optimize is

$$\mathcal{F} = \int dy |\phi(y)| T(y), \tag{31}$$

where $T(y)$ is the target displacement-amplitude distribution. As before, we aim to find an analytic expression for the gradient of this figure of merit in terms of a forward

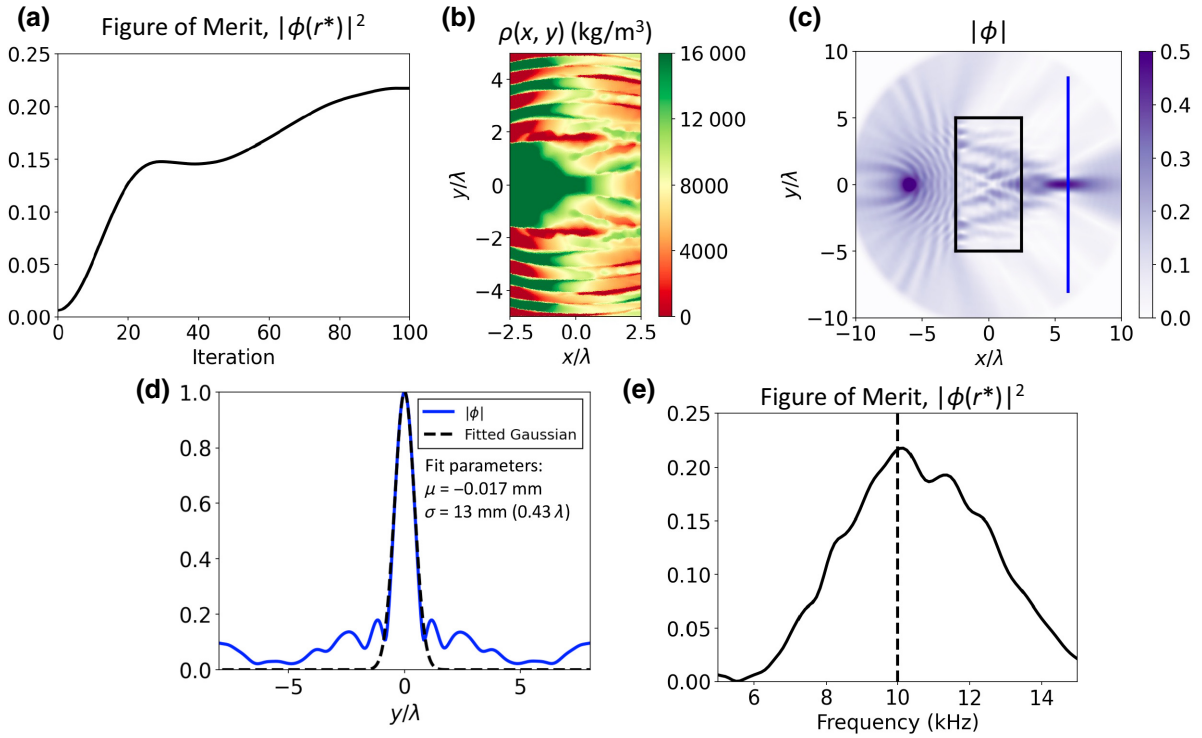

FIG. 6. A graded-density lens, designed using the adjoint method. (a) The change in the figure of merit, $|\phi(\mathbf{r}_*)|^2$, over the optimization. (b) The final mass density, $\rho(x,y)$ (kg/m^3). For reference, the initial mass density was that of steel, approximately 8000 kg/m^3. (c) The displacement amplitude $|\phi|$ of the final device. (d) A plot of the field along the cut line indicated by a blue line in (c), where we find that the width of the focus is 0.43λ. (e) The performance of the lens as a function of the frequency indicates a full-width-at-half-maximum bandwidth of approximately 5 kHz.

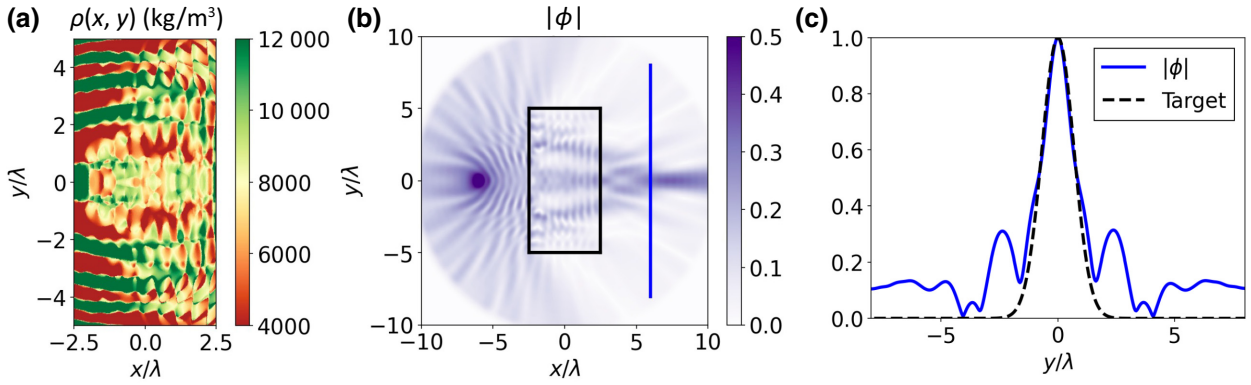

FIG. 7. Mode shaping with a graded plate. (a) Aiming to create a particular field distribution, the adjoint method is applied to design the density grading $\rho(x,y)$ (kg/m^3) as shown. (b) The displacement amplitude $|\phi|$ of the device. (c) A cut of the field along the line on which the amplitude has been designed.

field and an adjoint field. To this end, we expand the modulus of the displacement field under small perturbations,

$$|\phi+\delta\phi| = \sqrt{(\phi^*+\delta\phi^*)(\phi+\delta\phi)}, \tag{32}$$

$$= |\phi|\sqrt{1+\frac{2\mathrm{Re}[\phi^*\delta\phi]}{|\phi|^2}}, \tag{33}$$

$$\approx |\phi| + \frac{1}{|\phi|}\mathrm{Re}[\phi^*\delta\phi], \tag{34}$$

finding that the first-order correction is

$$\delta|\phi(y)| = \frac{1}{|\phi(y)|}\mathrm{Re}[\phi^*(y)\delta\phi(y)]. \tag{35}$$

Substituting this back into the figure-of-merit equation [Eq. (31)], the first-order change to the figure of merit is

$$\delta\mathcal{F} = \mathrm{Re}\left[\int dy \frac{1}{|\phi(y)|}T(y)\phi^*(y)\delta\phi(y)\right], \tag{36}$$

$$= \frac{h\omega^2}{D}\mathrm{Re}\left[\int dy \frac{1}{|\phi(y)|}\phi^*(y)G(y,\mathbf{r}_i)\phi(\mathbf{r}_i)T(y)\right]\Delta\rho. \tag{37}$$

Exploiting reciprocity to swap the arguments of the Green's function, we can identify the adjoint field as

$$\phi_{\mathrm{adjoint}}(\mathbf{r}) = \frac{h\omega^2}{D}\int dy \frac{\phi^*(y)}{|\phi(y)|}G(\mathbf{r},y)T(y), \tag{38}$$

so that the gradient of the figure of merit is given by $\partial\mathcal{F}/\partial\rho = \mathrm{Re}[\phi(\mathbf{r}) \times \phi_{\mathrm{adjoint}}(\mathbf{r})]$. At this point, we note that the adjoint field has a simple physical interpretation. The solution to a inhomogeneous differential equation can be found by integrating the source term against the Green's

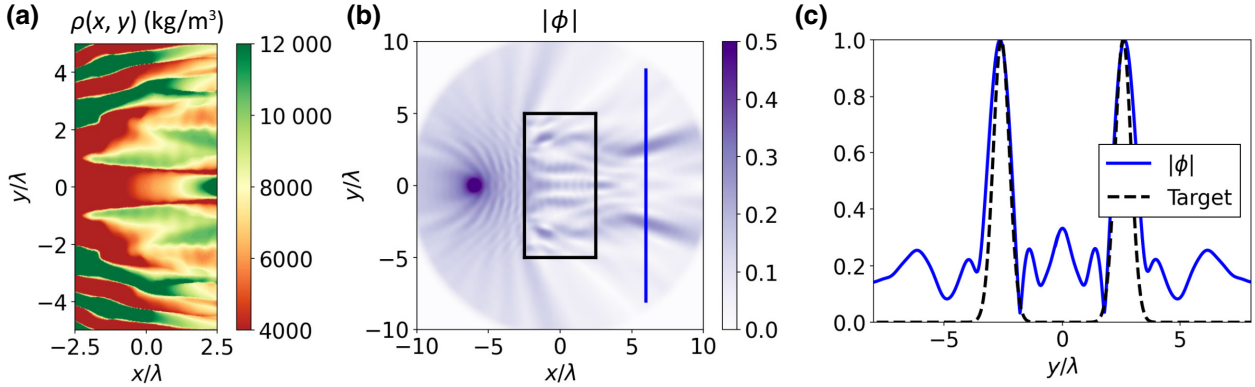

FIG. 8. A graded plate with a designed displacement-amplitude distribution along $x = 6\lambda$. (a) The density grading, $\rho(x,y)$ (kg/m^3). (b) The displacement amplitude, $|\phi|$. (c) A plot along the $x = 6\lambda$ line.

function. We can therefore conclude, based on the form of Eq. (38), that the adjoint field is generated by a distributed source given by the field distribution that we are aiming for, $T(y)$, up to a phase factor given by $\phi^*(y)/|\phi(y)|$. This has been noted before in the design of electromagnetic waveguide systems [30]. To shape the field in space, one must set up the adjoint source to be the desired field distribution and then solve the wave equation [Eq. (22)] to find the adjoint field. This is then interfered with the forward field to find how to grade the plate. An example of this is shown in Fig. 7, where the target displacement-amplitude distribution at $x = 6\lambda$ has been chosen to be

$$T(y) = \exp\left[-\frac{1}{2}\left(\frac{y}{0.02}\right)^2\right]. \tag{39}$$

The resulting density grading is shown in Fig. 7(a), with the field distribution shown in Fig. 7(b). A cut of the field along with the target distribution is shown in Fig. 7(c). As another example, we choose the target distribution of the field to be

$$T(y) = \exp\left[-\frac{1}{2}\left(\frac{y-0.08}{0.015}\right)^2\right] + \exp\left[-\frac{1}{2}\left(\frac{y+0.08}{0.015}\right)^2\right]. \tag{40}$$

Using this as the adjoint source, the resulting device is shown in Fig. 8.

IV. CONCLUSIONS AND OUTLOOK

Motivated by the recent development of simple but versatile methods for designing electromagnetic materials, we have presented two perturbative methods for designing thin elastic plates for a range of applications. While flexural waves on thin elastic plates have been studied for many years, the question of how to structure plates to achieve various wave-shaping effects remains open. Here, we have developed an iterative method for deciding where to pin a thin plate for focusing mechanical energy or isolating regions of space. Next, we have applied the adjoint method to thin elastic plates, allowing the graded density of the height profiles to be found that focus energy or enable mode shaping. Both methods are applicable to a range of problems, from energy harvesting to vibration isolation. We have also noted that the devices based on multiple-scattering effects between many pinned points exhibit lower bandwidth than graded devices. This is due to the sensitivity of multiple-scattering effects to changes in scatterer positions.

The methods that we have presented are easily extendable to vector elasticity, where one could try to affect mode conversion or design materials that manipulate different polarizations in different ways. More exotic wave-scattering effects could also be achieved by building up a system of resonant elements with unusual properties, such as ones with negative effective density or stiffness.

All data and code created during this research are freely available at Ref. [42].

ACKNOWLEDGMENTS

J.R.C. would like to thank Dr. G. J. Chaplain and Professor S. A. R. Horsley for many useful discussions and for their feedback on the manuscript. We acknowledge financial support from the Engineering and Physical Sciences Research Council (EPSRC) of the United Kingdom, via the EPSRC Centre for Doctoral Training in Metamaterials (Grant No. EP/L015331/1) and from the Defence Science Technology Laboratory (DSTL).

[1] D. S. Ballantine, S. J. Martin, A. J. Ricco, G. C. Frye, H. Wohltjen, R. M. White, and E. T. Zellers, *Acoustic Wave Sensors: Theory, Design, and Physico-Chemical Applications* (Academic Press, San Diego, 1997).

[2] G. Lee, D. Lee, J. Park, Y. Jang, M. Kim, and J. Rho, Piezoelectric energy harvesting using mechanical metamaterials and phononic crystals, Commun. Phys. **5**, 94 (2021).

[3] G. J. Chaplain, D. Pajer, J. M. De Ponti, and R. V. Craster, Delineating rainbow reflection and trapping with applications for energy harvesting, New J. Phys. **22**, 063024 (2020).

[4] R. Zhu, X. N. Liu, G. K. Hu, C. T. Sun, and G. L. Huang, A chiral elastic metamaterial beam for broadband vibration suppression, J. Sound Vib. **33**, 2759 (2014).

[5] D. Torrent, D. Mayou, and J. Sánchez-Dehesa, Elastic analog of graphene: Dirac cones and edge states for flexural waves in thin plates, Phys. Rev. B **87**, 115143 (2013).

[6] G. J. Chaplain, I. R. Hooper, A. P. Hibbins, and T. A. Starkey, Reconfigurable Elastic Metamaterials: Engineering Dispersion with Beyond Nearest Neighbors, Phys. Rev. Appl. **19**, 044061 (2023).

[7] M. Martí-Sabaté and D. Torrent, Edge modes for flexural waves in quasi-periodic linear arrays of scatterers, APL Mater. **9**, 081107 (2021).

[8] L. D. Landau and E. M. Lifshitz, *The Theory of Elasticity* (Butterworth Heinemann, Oxford, 1986), 3rd ed.

[9] A. N. Norris and C. Vemula, Scattering of flexural waves on thin plates, J. Sound Vib. **181**, 115 (1995).

[10] P. Packo, A. N. Norris, and D. Torrent, Metaclusters for the Full Control of Mechanical Waves, Phys. Rev. Appl. **15**, 014051 (2021).

[11] K. Jose, N. Ferguson, and A. Bhaskar, Branched flows of flexural waves in non-uniform elastic plates, Commun. Phys. **5**, 152 (2022).

[12] P. Packo, A. N. Norris, and D. Torrent, Inverse Grating Problem: Efficient Design of Anomalous Flexural Wave Reflectors and Refractors, Phys. Rev. Appl. **11**, 014023 (2019).

[13] G. J. Chaplain, J. M. De Ponti, G. Aguzzi, A. Colombi, and R. V. Craster, Topological Rainbow Trapping for Elastic Energy Harvesting in Graded Su-Schrieffer-Heeger Systems, Phys. Rev. Appl. **14**, 054035 (2020).
[14] L. Cao, Z. Yang, Y. Xu, S.-W. Fan, Y. Zhu, Z. Chen, B. Vincent, and B. Assouar, Disordered Elastic Metasurfaces, Phys. Rev. Appl. **13**, 014054 (2020).
[15] L. He, Z. Wen, Y. Jin, D. Torrent, X. Zhuang, and T. Rabczuk, Inverse design of topological metaplates for flexural waves with machine learning, Mater. Des. **199**, 109390 (2021).
[16] U. Leonhardt and T. Philbin, *Geometry and Light: The Science of Invisibility* (Dover, New York, 2010).
[17] S. Brûlé, E. H. Javelaud, S. Enoch, and S. Guenneau, Experiments on Seismic Metamaterials: Molding Surface Waves, Phys. Rev. Lett. **112**, 133901 (2014).
[18] M. Farhat, S. Guenneau, and S. Enoch, Ultrabroadband Elastic Cloaking in Thin Plates, Phys. Rev. Lett. **103**, 024301 (2009).
[19] N. Stenger, M. Wilhelm, and M. Wegener, Experiments on Elastic Cloaking in Thin Plates, Phys. Rev. Lett. **108**, 014301 (2012).
[20] M. Farhat, S. Guenneau, S. Enoch, and A. B. Movchan, Cloaking bending waves propagating in thin elastic plates, Phys. Rev. B **79**, 033102 (2009).
[21] D. J. Colquitt, M. Brun, M. Gei, A. B. Movchan, N. V. Movchan, and I. S. Jones, Transformation elastodynamics and cloaking for flexural waves, J. Mech. Phys. Solids **72**, 131 (2014).
[22] M. Rossi, D. Veber, and M. Gei, Numerical assessment of the performance of elastic cloaks for transient flexural waves, Front. Mater. **7**, 603667 (2020).
[23] M. Liu and W. D. Zhu, Nonlinear transformation-based broadband cloaking for flexural waves in elastic thin plates, J. Sound Vib. **445**, 270 (2019).
[24] A. Zareei and M.-Reza Alam, Broadband cloaking of flexural waves, Phys. Rev. E **95**, 063002 (2017).
[25] A. Darabi, A. Zareei, M.-Reza Alam, and M. J. Leamy, Experimental Demonstration of an Ultrabroadband Nonlinear Cloak for Flexural Waves, Phys. Rev. Lett. **121**, 174301 (2018).
[26] Y. Jin, B. Djafari-Rouhani, and D. Torrent, Gradient index phononic crystals and metamaterials, Nanophotonics **8**, 685 (2019).
[27] A. Climente, D. Torrent, and J. Sánchez-Dehesa, Gradient index lenses for flexural waves based on thickness variations, Appl. Phys. Lett. **105**, 064101 (2014).
[28] J. R. Capers, S. J Boyes, A. P. Hibbins, and S. A. R. Horsley, Designing the collective non-local responses of metasurfaces, Commun. Phys. **4**, 209 (2021).
[29] J. R. Capers, S. J Boyes, A. P. Hibbins, and S. A. R. Horsley, Designing disordered multi-functional metamaterials using the discrete dipole approximation, New J. Phys. **24**, 113035 (2022).
[30] C. M. Lalau-Keraly, S. Bhargava, O. D. Miller, and E. Yablonovitch, Adjoint shape optimization applied to electromagnetic design, Opt. Express **21**, 21693 (2013).
[31] P. M. Morse and K. U. Ingard, *Theoretical Acoustics* (McGraw-Hill, New York, 1968).
[32] D. V. Evans and R. Porter, Penetration of flexural waves through a periodically constrained thin elastic plate in vacuo and floating on water, J. Eng. Math. **58**, 317 (2007).
[33] L. L. Foldy, Multiple scattering theory of waves, Phys. Rev. **67**, 107 (1945).
[34] I. M. Gel'fand and N. Ya. Vilenkin, *Generalized Functions Vol. 1: Properties and Operations* (Academic Press, New York, 1964).
[35] S. Sra, S. Nowozin, and S. J. Wright, *Optimization for Machine Learning* (The MIT Press, Cambridge, Massachusetts, 2012).
[36] R. Storn and K. Price, Differential evolution—a simple and efficient heuristic for global optimization over continuous spaces, J. Glob. Optim. **11**, 314 (1997).
[37] W. T. Chen, A. Y. Zhu, V. Sanjeev, M. Khorasaninejad, Z. Shi, E. Lee, and F. Capasso, A broadband achromatic metalens for focusing and imaging in the visible, Nat. Nanotechnol. **13**, 220 (2018).
[38] A. Nagarajan, K. Vivek, M. Shah, V. G. Achanta, and G. Gerini, A broadband plasmonic metasurface superabsorber at optical frequencies: Analytical design framework and demonstration, Adv. Opt. Mater. **6**, 1800253 (2018).
[39] M. P. Bendsøe and O. Sigmund, *Topology Optimization: Theory, Methods and Applications* (Springer, Berlin, 2003).
[40] P. M. Morse and H. Feshbach, *Methods of Theoretical Physics* (McGraw-Hill, New York, 1953).
[41] COMSOL MULTIPHYSICS v. 6.1. www.comsol.com. comsol ab, stockholm, sweden.
[42] https://doi.org/10.24378/exe.4785.